Nephrol Dial Transplant (2004) 19: 1708–1715
DOI: 10.1093/ndt/gfh275
Advance Access publication 18 May 2004

Original Article

Nephrology
Dialysis
Transplantation

Neutrophil contribution to the crescentic glomerulonephritis in SCG/Kj mice

Akiko Ishida-Okawara[1], Toshiko Ito-Ihara[1,2], Eri Muso[3], Takahiko Ono[2], Kan Saiga[4], Kyuichi Nemoto[4] and Kazuo Suzuki[1]

[1]Biodefense Laboratory, National Institute of Infectious Diseases, Toyama 1-23-1, Shinjuku-ku, Tokyo 162-8640, Japan, [2]Nephrology Division, Department of Cardiovascular Medicine, Graduate School of Medicine, Kyoto University, Kawara-cho 54, Shogoin, Sakyou-ku, Kyoto 606-8507, Japan, [3]Division of Nephrology and Dialysis, Kitano Hospital, The Tazuke Kofukai Medical Research Institute, 2-4-20 Ohgimachi, Kita-ku, Osaka 530-8480, Japan and [4]Nippon Kayaku Co. Ltd, 31-12, Shimo, 3-chome, Kita-ku 115-8588, Japan

Abstract

Background. Myeloperoxidase-specific anti-neutrophil cytoplasmic auto-antibody (MPO-ANCA) has been a useful diagnostic marker in systemic vasculitis with crescentic glomerulonephritis (CrGN). It is highly suspected that the antigenic enzyme MPO released from activated neutrophils is involved in these lesions. We evaluated the relationship between neutrophil functions including peripheral neutrophil counts and renal lesions in SCG/Kj mice as a model of ANCA-associated CrGN and vasculitis.

Methods. Peripheral neutrophil counts, the plasma levels of MPO-ANCA and tumour necrosis factor alpha (TNF-α) were measured. The capacity of MPO release and superoxide generation were evaluated as neutrophil activity. The renal lesions were estimated by grade of proteinuria, histopathological lesion, such as glomerular neutrophil infiltration and active or chronic renal injury scores with crescent formation.

Results. MPO-ANCA and TNF-α levels were higher than those of normal mice C57BL/6 even before overt proteinuria; subsequently, peripheral neutrophils increased. In the phase of nephritis with low grade proteinuria, the spontaneous release of MPO from peripheral neutrophils increased, while superoxide generation increased before spontaneous MPO release occurred. In addition, the renal lesion in histological observations was aggravated with ageing and the glomerular neutrophil infiltration was positively correlated with MPO-ANCA levels, as well as with histological indices of nephritis, active renal injury score; in particular, crescent formation was correlated with spontaneous MPO release. In contrast, superoxide generation was negatively correlated with the severity of this lesion during the progression.

Conclusions. These findings indicate that neutrophils are activated and contribute to the development of the active crescentic lesion in SCG/Kj mice.

Keywords: activated neutrophils; crescentic glomerulonephritis; MPO-ANCA; SCG/Kj mice; TNF-α

Introduction

In acute inflammatory disorders, multiple pathological processes are linked to the ability of neutrophils to release a complex assortment of agents that can destroy normal cells and dissolve connective tissue. As one of these agents, reactive oxygen intermediates (ROI) have been known to have a potential for tissue destruction [1]. In the presence of neutrophil-derived myeloperoxidase (MPO), even small amounts of ROI generate hypochlorus acid and then initiate the deactivation of antiproteases or activation of latent proteases, which lead to tissue damage if not properly controlled.

Antibodies directed against cytoplasmic constituents of the neutrophilic granulocyte have been extensively described as markers for systemic vasculitis and crescentic glomerulonephritis (CrGN) [2]. It has also been shown that MPO and the MPO-specific anti-neutrophil cytoplasmic auto-antibody (MPO-ANCA) are risk factors for the development of these lesions, possibly through ROI production as described above. In the sera of patients with microscopic polyangiitis [3] and CrGN [2], high titres of MPO-ANCA are frequently detected. Although it has been demonstrated

Correspondence and offprint requests to: Kazuo Suzuki, PhD, Chief of Biodefense Laboratory, National Institute of Infectious Diseases (NIID-NIH), Toyama 1-23-1, Shinjuku-ku, Tokyo, 162-8640, Japan. Email: ksuzuki@nih.go.jp. The authors wish it to be known that, in their opinion, the first two authors should be regarded as joint First Authors.

the role of neutrophil activation and MPO-ANCA as the initial risk of these lesions, it is necessary to investigate the precise network between neutrophils activation and development of CrGN.

As the basis for clinical studies, animal models are often used to understand the mechanisms of the development of vasculitis, and to establish therapeutic strategies. Both MRL lpr/lpr [4] and SCG/Kj [5] strains are known to show high levels of MPO-ANCA in association with renal lesions, including glomerulonephritis (GN) and vasculitis. Recently, using MPO KO mice we have clarified that MPO is a major antigen for MPO-ANCA production [6]. Moreover, the study using NZB/W F1 mice with the Fcg receptor deficiency has shown that the Fcg receptor on neutrophils and/or macrophages is necessary for the occurrence of GN [7]. Recently, using $Rag2^{-/-}$ and C57BL/6J mice, Xiao *et al.* [8] have demonstrated that anti-MPO IgG antibodies cause pauci-immune glomerular necrosis and crescent formation both in the presence or absence of functional T or B lymphocytes. Other studies have identified the gene responsible for GN and vasculitis [9]. However, the more precise pathogenic roles of MPO-ANCA and neutrophils in the development of GN and vasculitis in these murine models are undetermined.

In the present study, using SCG/Kj mice, a model of spontaneous CrGN and vasculitis, the role of activated neutrophils in the development of nephritis was investigated by evaluating the relationship between neutrophil function and renal lesions.

Subjects and methods

Mice

Female C57BL/6 mice were purchased from SLC Corporation (Shizuoka, Japan). Female SCG/Kj mice were bred and maintained at the animal facility of Nippon Kayaku Co. Ltd. Both mouse strains were maintained under specific pathogen-free conditions, and treated according to guidelines for animal care.

Reagents

fMet-Leu-Phe (FMLP) was purchased from Peptide Institute (Osaka, Japan). 3,3′, 5,5′-Tetramethylbendizine (TMB), cytochalasin B (CB), cytochrome *c* and phosphatase substrate were obtained from Sigma Chemical Company (St Louis, MO, USA). Alkaline phosphatase (AP)-labeled anti-mouse IgG was purchased from Cappel Corporation (West Chester, PA, USA), AP-labeled anti-human IgG antibody was purchased from Bio-Rad Corporation (Hercules, CA, USA). A kit for mouse TNF-α immunoassay was purchased from R & D Systems (Minneapolis, MN, USA). Nycoprep and 1 Step Polymorphs, for preparation of blood cells, were obtained from Nycomed Pharma AS (Oslo, Norway) and Chemical and Scientific Corporation (Osaka, Japan), respectively. Urine biochemical assay sticks were purchased from Bayel Medical Corporation (Tokyo, Japan). PQE-30, restriction enzymes and Ligation High were purchased from Qiagen (Hilden, Germany), TaKaRa (Shiga, Japan) and Toyobo (Osaka, Japan), respectively.

Grouping of SCG/Kj mice according to proteinuria

SCG/Kj mice were divided into three groups depending on the grades of proteinuria because proteinuria is one of the reliable indices of renal damage and the severity of GN in these mice did not always synchronize with age. Haematuria is often used as a marker of active CrGN in human cases, however, in the present study, proteinuria was employed as a marker of the severity of nephritis because the mice died at the onset of haematuria.

Proteinuria was determined by using a clinical stick as a marker for the onset and development of nephritis. In this study, the 'initial' phase was defined as below 30 mg/dl of proteinuria ($n=6$, age 8.2 ± 0.4 weeks), the 'early' phase of nephritis was defined as 30–300 mg/dl ($n=18$, age 12.7 ± 2.1 weeks) and the 'late' phase of nephritis was defined as over 300 mg/dl ($n=21$, age 13.1 ± 1.3 weeks), respectively. The damage to the renal lesion of the mice showed heterogeneity not dependent on their age. C57BL/6 mice of 9 and 14 weeks of age were used as normal mice.

Preparation of recombinant mouse MPO (rmMPO) and antibody to rmMPO

rmMPO was prepared by the expression in *Escherichia coli* transfected with a plasmid containing cDNA of mouse MPO. The cDNA pool was obtained from bone marrow cells of C57BL/6 mice by a PCR technique and ligated into an expression vector pQE-30. The mouse MPO cDNA was amplified by PCR from the cDNA pool using Platinum *Taq* DNA polymerase High Fidelity (Life Technologies, PTC-200; MJ Research, Waltham, MA, USA) using a ThermoScript RT-PCR System (Invitrogen Corp., Carlsbad, CA, USA). The MPO cDNA sequence we amplified was different from GenBank X15313 at 27 sites for six positions in the amino acid (Figure 1a). It was ligated in an expression vector pQE-30 between the BamHI site and the HindIII site. We transformed the plasmid into a host *E.coli* SG13009[pREP4] (Qiagen, Tokyo, Japan). The expressed protein consisted of His-tag-L-chain-H-chain of mouse MPO (Figure 1b). The bacteria were cultured in a medium containing Terrific Broth, 100 mg/ml ampicillin and 25 mg/ml kanamycin until ~4.6 of absorbance at 600 nm after addition of isopropyl-β-D-thiogalactopyranoside (IPTG), then we obtained with higher yield of rmMPO. The bacteria were lysed by sonication in 6 M guanidine–hydrogen chloride and then we purified the recombinant protein with affinity chromatography using a Ni-attached gel (Ni-NTA agarose; Qiagen) in 8 M urea, as described elsewhere [10] (Figure 1c). The IgG fraction of the polyclonal antibody to mouse MPO was prepared from serum of rabbit immunized with rmMPO and purified with Protein A (Pharmacia Fine Chemicals, Uppsala, Sweden) (Figure 1d). In addition, to evaluate the MPO-ANCA titre as equivalent to human MPO-ANCA, human MPO III was isolated from neutrophils of healthy volunteers, as previously described [11]. Briefly, neutrophils were extracted by detergents and purified by a series of DEAE and CM chromatography steps and HPLC. The completely purified sample had a Reinheitzahl (Rz) value, with an absorbance ratio of 430 to 280 nm of >0.7.

Measurement of MPO-ANCA levels in sera by ELISA

Sera were prepared from the abdominal aorta blood of the mice. MPO-ANCA levels were measured as described

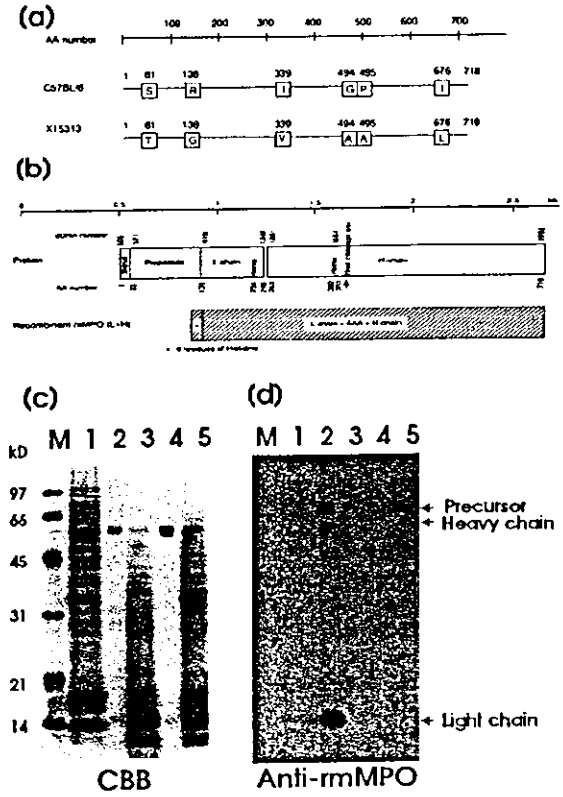

Fig. 1. Preparation of anti-rmMPO by rmMPO and evaluation of the antibody with western blotting. (a) Structure difference in mouse MPO between X15313 in GenBank and C57BL/6. (b) Construction of rmMPO. (c) Proteins in purification step. M, marker; 1, mouse neutrophils; 2, purified native mouse MPO; 3, human neutrophils; 4, purified human MPO; 5, human mononuclear cells; CBB, Coomassie brilliant blue stain.

previously [6]. Briefly, human MPO III was coated onto an ELISA plate (TS plate; Toyoshima Co., Tokyo, Japan) overnight at 4°C. The plate was blocked and mouse serum (×50 dilution) was added for 1.5 h at room temperature. AP-labeled anti-mouse IgG antibody (×1000 dilution) or an AP-labeled anti-human IgG antibody (×3000 dilution) was added and allowed to react for 2 h at room temperature. Afterwards, *p*-nitrophenylphosphate, an AP substrate, was added at a concentration of 1 mg/ml. After incubation at room temperature, the absorbance at 405 nm was measured by a model LFA-096 automatic analyser. The titre of MPO-ANCA in mouse sera was determined with human standard serum to obtain the human ELISA unit equivalent (hEU).

Measurement of TNF-μ in plasma

The diluted plasma (50 ml) was added to the each well of a 96 well F-plate and incubated for 2 h at room temperature. Each well was aspirated and washed five times; subsequently, 100 μl of conjugate was added to each well and incubated for 2 h at room temperature. This process was repeated with a 30 min incubation period upon addition of the substrate solution. Finally, 100 μl of stop solution was added to each well and absorbance measured at 450 nm.

Preparation of peripheral neutrophils of SCG/Kj mice

Heparinized blood, taken from the abdominal aorta of the mouse, was put onto the continuous preparation reagents, which consisted of 1.5 ml of Nycoprep, with a density of 1.077, added to 1.5 ml of 1 Step Polymorphs with a density of 1.113, and subsequently centrifuged for 30 min at 600 *g* at 20°C. Neutrophils were obtained in the layer between the two reagents. Erythrocytes contained in the neutrophil fraction were lysed to obtain the neutrophils. Confirmation of over 85% yield of neutrophils was demonstrated by staining with a peroxidase detection kit (Muto Pure Chemicals Co., Ltd, Tokyo, Japan). Cell viability >99% was detected by trypan blue dye exclusion.

Measurement of MPO release and superoxide generation of neutrophils

Neutrophil degranulation, measurement of MPO release and superoxide generation were performed as described previously [12]. Briefly, neutrophils, which were pre-warmed for 10 min at 37°C, were stimulated in the presence or absence of CB and FMLP in a 96 well V-plate for 10 min at 37°C. After incubation, the plate was immersed in ice and then centrifuged at 350 *g* for 5 min at 4°C to separate the supernatant from the cell pellet. MPO activity in the supernatant and cell lysate was assayed by the TMB method, as described previously [12]. Superoxide generation of neutrophils was determined by measuring the reduction of cytochrome *c*.

Histological examination of glomeruli

Haematoxylin–eosin and periodic acid-Schiff (PAS) staining. Kidneys were removed, fixed with buffered formalin, and embedded in paraffin. To assess the activity and chronicity of the lesions in SCG/Kj mice, serial 4 μm sections were stained with haematoxylin–eosin and periodic acid-Schiff.

Immunoperoxidase staining for neutrophils. Neutrophils were confirmed by an indirect method using a polyclonal rabbit antibody against rmMPO as described previously [13]. Briefly, the sections were incubated with the primary antibody followed by biotinylated anti-rabbit IgG (Vector Laboratories, Burlingame, CA, USA). The sections were then reacted with avidin-DH-biotinylated horseradish peroxidase complex (Vectastain ABC kit; Vector Laboratories). Colour was then developed by incubation with an ImmunoPure Metal Enhanced DAB Substrate kit (Pierce, Rockford, IL, USA).

Evaluation of renal lesion. The number of the infiltrated neutrophils into 20 glomeruli was counted based on nuclear morphology of HE and PAS staining. Matrix expansion was also measured. Moreover, each specimen was used to determine the activity index (AI) and chronicity index (CI) according to the modified NIH criteria by Austin *et al.* [14], originally developed for systemic lupus erythematosus, as follows. The AI was scored in the presence of cell proliferation, cellular and fibrocellular crescent formation, interstitial

mononuclear cell infiltration, and small vessel vasculitis. The presence of cell proliferation and interstitial mononuclear cell infiltration was scored in a range of 0–3 (0 = absent, 1 = mild, 2 = moderate and 3 = severe). The presence of cellular or fibrocellular crescents was scored in a range of 0–3 (0 = absent, 1 = <20% of the glomeruli involved, 2 = 20–50% glomeruli involved, 3 = >50% glomeruli involved). The maximal activity score amounted to 10. The CI scored the presence of matrix expansion (0–3), global glomerulosclerosis (0–3), and tubulointerstitial change such as tubular atrophy and/or interstitial fibrosis (0–3). The maximal chronicity index amounted to 12. The crescent score was evaluated by the modified method of Floege [15] as follows: 40 glomerular cross-sections were graded by a relative area of the cellular crescent occupied in Bowman's capsule as 0, negative; 1, 1–25%; 2, 26–50%; 3, 51–75%; 4, 76–100%; and then the total grade in 40 glomeruli was defined as the crescent score.

Statistical analysis

Values were expressed as mean ± SD and were analysed for statistical differences by the Mann–Whitney *U*-test. Correlations were analysed by the Pearson test. The probability value of <0.05 was considered significant.

Results

The changes of neutrophil counts, MPO-ANCA levels and TNF-α in peripheral blood related with the nephritis development

The peripheral neutrophil count did not increase in C57BL/6 mice with ageing. In SCG/Kj mice, the count was significantly elevated in the early phase. It also increased in the late phase. As a result, peripheral neutrophil counts in both early and late phases significantly increased compared with those of control C57BL/6 mice and in the initial phase of SCG/Kj mice (Figure 2a).

The serum levels of MPO-ANCA in SCG/Kj mice in all phases of nephritis were higher than those in C57BL/6 mice (Figure 2b). Ratios of SCG/Kj mice showing MPO-ANCA positive in sera were 17.6% in the initial phase, 11.1% in the early phase and 20% in the late phase, respectively. Two mice showed positive values of MPO-ANCA without crescent formation (data not shown).

Plasma TNF-α levels of SCG/Kj mice were significantly higher than those in C57BL/6 mice, particularly in the early phase. The increase was significant, compared either with control mice or with the initial phase of nephritis in SCG/Kj mice (Figure 2c).

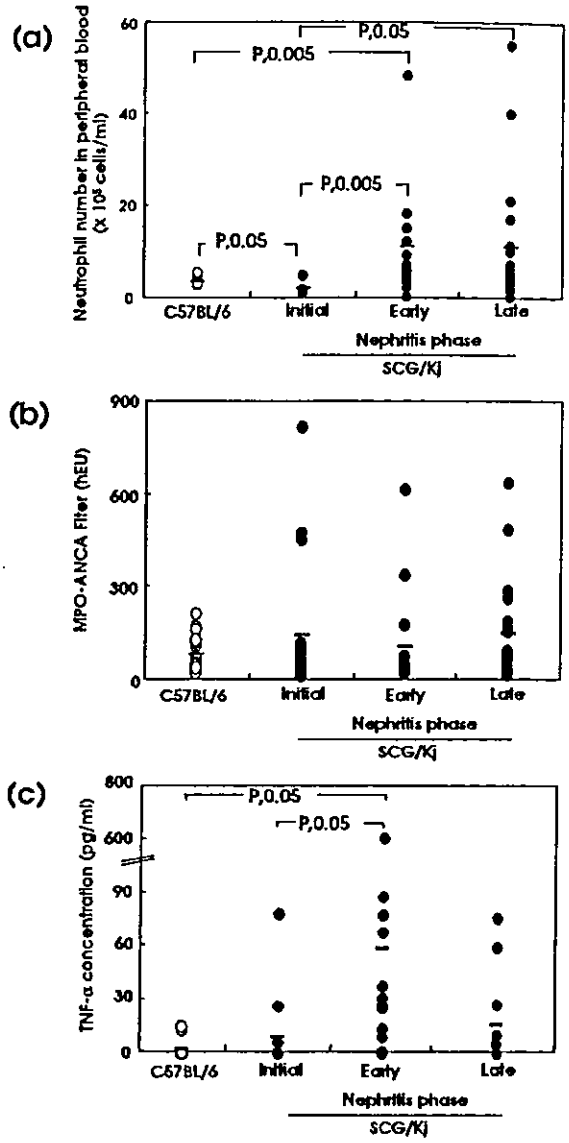

Fig. 2. Peripheral neutrophil counts and MPO-ANCA levels in the sera and plasma TNF-α concentrations in SCG/Kj mice. (a) Peripheral neutrophil counts. (b) MPO-ANCA levels in the sera. (c) TNF-α concentration in the plasma in SCG/Kj and C57BL/6 mice. The initial phase of nephritis: <30 mg/dl of proteinuria; the early phase of nephritis: 30–300 mg/dl of proteinuria; the late phase of nephritis: >300 mg/dl of proteinuria.

Neutrophil function in each phase of nephritis

Spontaneous and FMLP stimulated MPO release from peripheral neutrophil. In SCG/Kj mice, although spontaneous MPO release from peripheral neutrophils was relatively enhanced in the early phase of nephritis (Figure 3a), there was no marked difference in the levels. FMLP-induced MPO release showed no difference in all phases and between two strains of mice (Figure 3b).

Superoxide generation from peripheral neutrophils. Superoxide generation in SCG/Kj mice was higher than that of control mice. In particular, it was significantly enhanced in the initial phase of nephritis (Figure 3c).

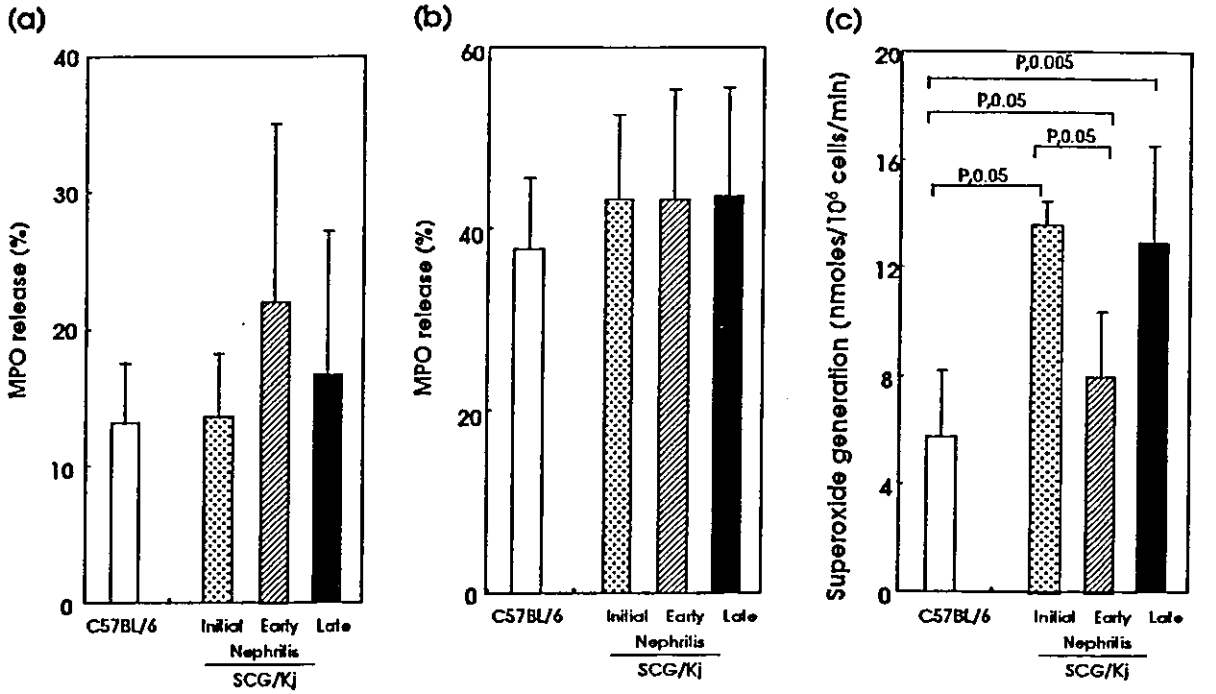

Fig. 3. Neutrophil activation in SCG/Kj mice. MPO release from neutrophils in SCG/Kj mice. Prewarmed neutrophils (10^6 cells/ml) were stimulated (a) in the absence or (b) presence of FMLP (10^{-5} M) and CB (5 μg/ml). (c) Superoxide generation in SCG/Kj and C57BL/6 mice.

Table 1. Renal lesion of SCG/Kj mice with ageing.

Age range (weeks)	Activity Index	Chronicity Index	Crescent formation (%)	Neutrophil infiltration (glomerulus)	Matrix expansion
8–9 (mean 8.17±0.41)	2.33±0.82	1.00±0	0.55±0.63	0.44±0.11	1.00±0
10–12 (mean 11.31±0.63)	3.77±1.09	2.15±0.38*	0.8±1.06	0.84±0.42	2.15±0.38*
13–16 (mean 13.96±0.89)	4.92±1.73*	2.64±1.32*	10.96±18.00	1.10±0.57*	2.08±0.49*

*$P < 0.05$

Renal lesion with ageing in histological findings of SCG/Kj mice

The changes of characteristics of renal lesion with ageing in SCG/Kj mice are shown in Table 1. Both AI and CI significantly increased depending on age (Table 1). Crescent formation markedly increased after ageing, although there was no statistical significance among ages. Any interstitial fibrosis was not detected but some global sclerosis was also detected in these mice (data not shown). Vasculitis was detected in two mice irrespective of age at 10 and 14 weeks (data not shown). Glomerular neutrophil infiltration significantly increased with the development after 13 weeks of age (Table 1). In severe nephritis with cellular crescent formation, marked infiltration was often observed in the glomeruli (Figure 4a). We confirmed neutrophils by staining with antibody against MPO (Figure 4b). Although matrix expansion significantly increased from 10 weeks of age, these increases did not enhance with ageing (Table 1).

Relationship between glomerular neutrophil infiltration and parameters of histological findings in SCG/Kj mice

Glomerular neutrophil infiltration correlated with the AI (Figure 5a), with the crescent formation score (Figure 5b) and with the CI ($R = 0.43$, $P < 0.01$, data not shown). In addition, it correlated with MPO-ANCA levels in sera (Figure 5c), although there was no direct relationship between serum levels of MPO-ANCA and crescent formation score.

Relationship between neutrophil function and histological lesions

We analysed the influence of neutrophil activity measured by spontaneous MPO release in the histological lesions in SCG/Kj mice. Spontaneous MPO release was positively correlated with not only crescent formation score (Figure 6a), but also the renal AI (Figure 6b) (crescent formation score, $R = 0.39$, $P < 0.05$; AI, $R = 0.32$, $P < 0.05$). This correlation was

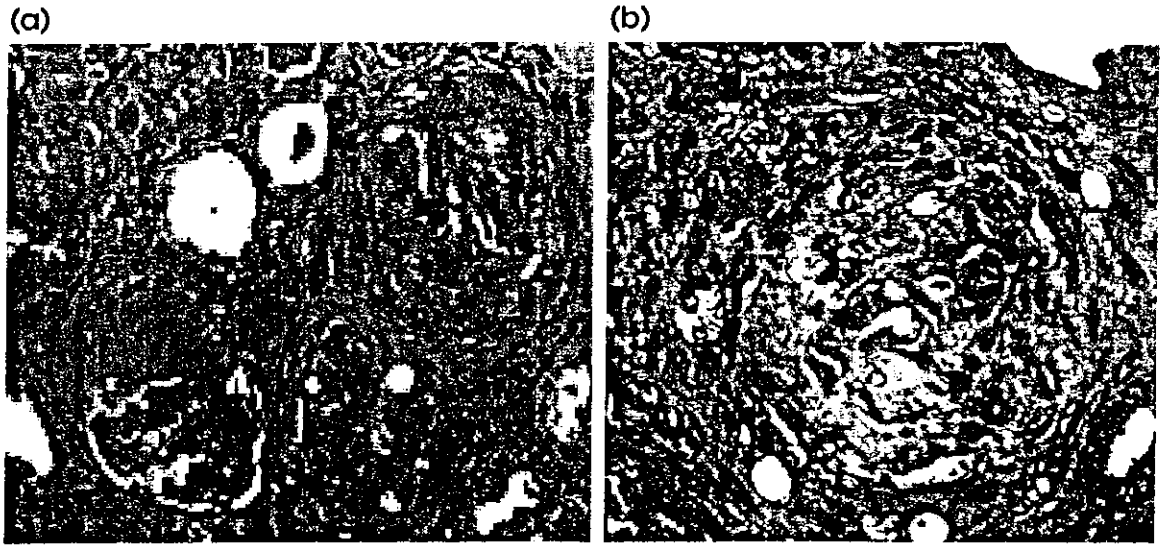

Fig. 4. Renal histological analysis in SCG/Kj mice. Correlation between neutrophil infiltration into the glomeruli and renal injury. (a) Light microscopy of infiltrated neutrophils into the glomeruli in the late phase of nephritis. Periodic acid-Schiff staining were performed (final magnification ×200). (b) Neutrophils, which were positive for rmMPO staining, were abundantly observed in the tissue from the late phase of nephritis (final magnification ×400).

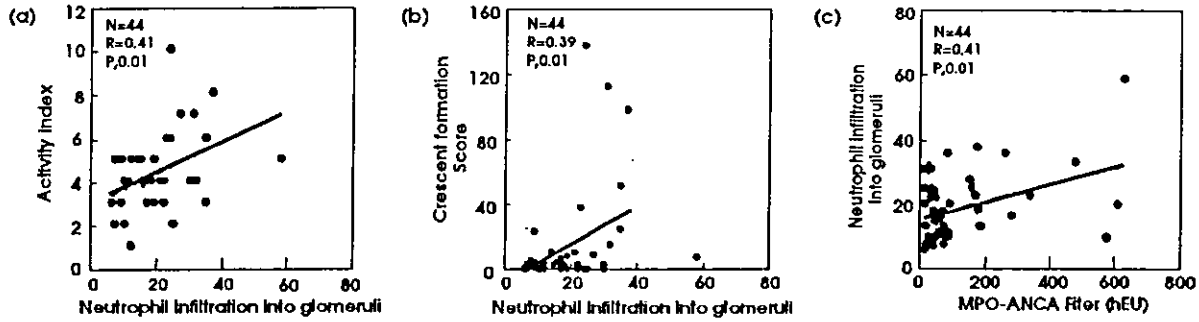

Fig. 5. Correlation between neutrophil infiltration into the glomeruli and renal injury in SCG/Kj mice. (a) Correlation between neutrophil infiltration into the glomeruli and AI ($n=44$, $R=0.41$, $P<0.01$). (b) Correlation between neutrophil infiltration into the glomeruli and the crescent formation score ($n=44$, $R=0.39$, $P<0.01$). (c) Correlation between neutrophil infiltration into the glomeruli and MPO-ANCA levels ($n=44$, $R=0.41$, $P<0.01$).

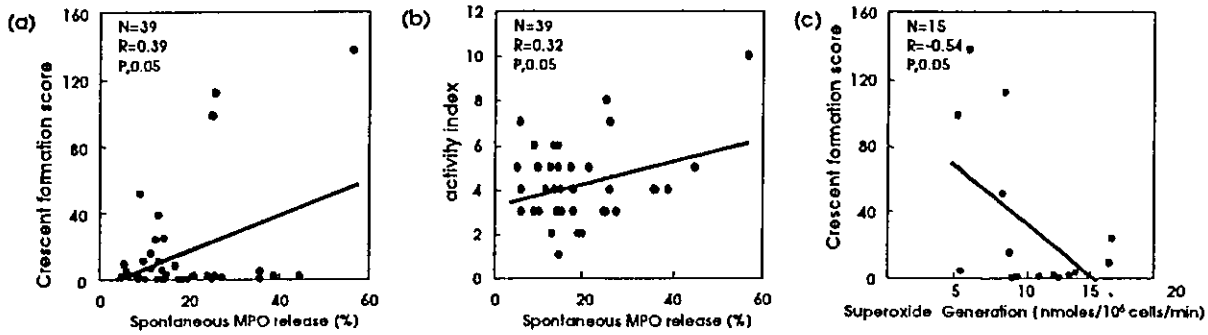

Fig. 6. Correlation between neutrophil activation and renal injury in SCG/Kj mice. (a) Correlation between spontaneous MPO release and crescent formation score AI in the early phase ($n=39$, $R=0.39$, $P<0.05$). (b) Correlation between spontaneous MPO release and AI ($n=39$, $R=0.32$, $P<0.05$). (c) Negative correlation between superoxide generation and the crescent formation score ($n=15$, $R=-0.54$, $P<0.05$)

also obtained with the renal CI ($R = 0.32$, $P < 0.05$, data not shown). On the other hand, a negative correlation was noted between superoxide generation and crescent formation score (Figure 6c).

Discussion

Rapidly progressive glomerulonephritis (RPGN) is a severe form of immune-mediated renal disease that is often poorly responsive to therapy [16]. SCG/Kj mice have been reported as a potent animal model for human RPGN [5,17,18]. In the original report, 58% of female mice revealed RPGN [17]. As shown in our study, marked crescent formation was detected in their renal tissue associated with a variety of proteinuria from a relatively early age.

In the present study, we examined the contribution of activated neutrophils to the development of nephritis in this strain of mice. As the development of renal lesions showed marked heterogeneity, independent of age, we classified its severity of nephritis into three phases (initial, early and late phases) depending on the grade of proteinuria.

The number of mice with a high peripheral neutrophil count increased along with the severity of nephritis. In all phases of nephritis, MPO-ANCA levels in sera were higher in SCG/Kj mice than those in control mice, although a statistical difference could not be obtained. These observations in mice are similar to that of the patient with RPGN.

TNF-α levels in plasma significantly increased in the early phase of nephritis in SCG/Kj mice. Dewas *et al.* [19] have recently reported that TNF-α, via its p55 receptor, induces protein tyrosine kinase-dependent selective phosphorylation of $p47^{phox}$ on specific serines in human neutrophils. On the other hand, Timoshanko *et al.* [20] have reported that intrinsic renal cells are the major cellular source of TNF-α contributing to inflammatory injury in CrGN. These findings suggest that neutrophils primed with TNF-α produce superoxide through activation of NADPH oxidase. Based on our data, elevation of superoxide generation in the initial phase was coincident with higher levels of TNF-α in the plasma. These observations suggest that in the initial phase of CrGN, peripheral neutrophils may be activated with TNF-α priming. Subsequently, activated neutrophils showed a release of MPO without stimulation in the early phase, but superoxide generation was already activated in the initial phase, suggesting that activated neutrophils are easy to degranulation with no stimulation. In addition, decrease of superoxide generation in the early phase may be a result of suppression of the cascade of NADPH oxidase activation, which occurs due to desensitization of neutrophils after the initial phase. Higher counts of activated neutrophils in peripheral blood from early phase to late phase may cause damage to endothelial cells, resulting in the vascular lesion involved in CrGN. Indeed, spontaneous MPO release from peripheral neutrophils was correlated with the crescent formation score, AI and CI, but negative correlation in superoxide generation, suggesting activated neutrophils cause the renal lesion.

A correlation between glomerular neutrophil infiltration and increased MPO-ANCA levels was shown in SCG/Kj mice. This reflects the correlation between neutrophil activation and increased MPO-ANCA levels in the sera of patients with GN. Bajema *et al.* [21] reported co-localization of MPO and fibrinoid necrosis by using their double staining technique in ANCA-associated vasculitis. They have demonstrated that both neutrophils and liberated MPO exist in injured glomeruli tissue, suggesting that MPO may cause tissue damage by generating hypochlorous acid.

In addition, glomerular neutrophil infiltration was correlated with the crescent formation score, AI and CI. Miyazawa *et al.* [18] recently reported the important role of glomerular neutrophil influx as an initial response in the process of crescent formation in SCG/Kj mice. From these findings, neutrophil infiltration into glomeruli and MPO-ANCA production could be associated with the beginning of the renal lesion. On the other hand, MPO-ANCA production might be enhanced by the impaired clearance by apoptosis of activated or abnormal neutrophils, with or without other stimuli [22]. An increase of peripheral neutrophils escaping from apoptosis might directly injure renal tissue. Based on our data, MPO-ANCA production increased in the initial phase before elevation of proteinuria, suggesting that MPO-ANCA is a trigger for elevation of renal lesion. However, deposition of IgGs and complement 3 along peripheral capillary loops [5] and auto-antibodies against DNA and the glomerular basement membrane that are produced as a result of polyclonal B cell activation [4], could participate in pathogenesis of GN.

Neutrophils activated with TNF-α and MPO-ANCA may participate in the onset of CrGN by superoxide generation. Subsequently, degranulation, including MPO release, continuously damages the endothelium. Finally, constitutive neutrophil activation could be involved in active crescentic lesion of glomeruli in SCG/Kj mouse.

Acknowledgements. We thank Drs David Jayne, Consultant in Nephrology and Vasculitis, Addenbrookes Hospital, Cambridge, UK, Masahisa Kyogoku, Tohoku University School of Medicine, Sendai, Japan, Wayne K. Dawson and Amanda Persad, in NIID, Tokyo, Japan for their critical review of the manuscript. This work was supported in part by a grant for Researches of Measures for Intractable Diseases, Pharmaceutical and Medical Safety and Health Sciences focusing on Drug Innovation of Health and Labour Sciences Research Grants of Ministry of Health, Labour and Welfare.

Conflict of interest statement. None declared.

References

1. Johnson RJ, Couser WG, Chi EY *et al.* New mechanism for glomerular injury. Myeloperoxidase-hydrogen peroxide-halide system. *J Clin Invest* 1987; 79: 1379–1387

2. Arimura Y, Minoshima S, Kamiya Y *et al.* Serum myeloperoxidase and serum cytokines in anti-myeloperoxidase antibody-associated glomerulonephritis. *Clin Nephrol* 1993; 40: 256–264
3. Falk RJ, Nachman PH, Hogan SL *et al.* ANCA glomerulonephritis and vasculitis: a Chapel Hill perspective. *Semin Nephrol* 2000; 20: 233–243
4. Harper JM, Thiru S, Lockwood CM *et al.* Myeloperoxidase autoantibodies distinguish vasculitis mediated by anti-neutrophil cytoplasm antibodies from immune complex disease in MRL/Mp-lpr/lpr mice: a spontaneous model for human microscopic angiitis. *Eur J Immunol* 1998; 28: 2217–2226
5. Neumann I, Birck R, Newman M *et al.* SCG/Kinjoh mice: a model of ANCA-associated crescentic glomerulonephritis with immune deposits. *Kidney Int* 2003; 64: 140–148
6. Ishida-Okawara A, Oharaseki T, Takahashi K *et al.* Contribution of myeloperoxidase to coronary artery vasculitis associated with MPO-ANCA production. *Inflammation* 2001; 25: 381–387
7. Wakayama H, Hasegawa Y, Kawabe T *et al.* Abolition of anti-glomerular basement membrane antibody-mediated glomerulonephritis in FcRgamma-deficient mice. *Eur J Immunol* 2000; 30: 1182–1190
8. Xiao H, Heeringa P, Hu P *et al.* Antineutrophil cytoplasmic autoantibodies specific for myeloperoxidase cause glomerulonephritis and vasculitis in mice. *J Clin Invest* 2002; 110: 955–963
9. Wang Y, Nose M, Kamoto T *et al.* Host modifier genes affect mouse autoimmunity induced by the lpr gene. *Am J Pathol* 1997; 151: 1791–1798
10. Tomizawa K, Mine E, Fujii A *et al.* A panel set for epitope analysis of myeloperoxidase (MPO)-specific anti-neutrophil cytoplasmic antibody MPO-CA using recombinant hexamer histidine-tagged MPO deletion mutants. *J Clin Immunol* 1998; 18: 142–152
11. Suzuki K, Yamada M, Akashi K *et al.* Similarity of kinetics of three types of myeloperoxidase from human leukocytes and four types from HL-60 cells. *Arch Biochem Biophys* 1986; 245: 167–173
12. Ishida-Okawara A, Kimoto Y, Watanabe K *et al.* Purification and characterization of aseanostatins: actinomycete-derived fatty acid inhibitors to myeloperoxidase release from human polymorphonuclear leukocytes. *J Antibiot* 1991; 44: 524–532
13. Liu N, Ono T, Suyama K *et al.* Factor V expression colocalized with fibrin deposition in IgA nephropathy *Kidney Int* 2000; 58: 598–606
14. Austin HA 3rd, Muenz LR, Joyce KM *et al.* Prognostic factors in lupus nephritis. Contribution of renal histologic data. *Am J Med* 1983; 75: 382–391
15. Floege J, Johnson RJ, Gordon K. *et al.* Increased synthesis of extracellular matrix in mesangial proliferative nephritis. *Kidney Int* 1991; 40: 477–478
16. Zauner I, Bach D, Braun N *et al.* Predictive value of initial histology and effect of plasmapheresis on long-term prognosis of rapidly progressive glomerulonephritis. *Am J Kidney Dis* 2002; 39: 28–35
17. Kinjoh K, Kyogoku M, Good RA. Genetic selection for crescent formation yields mouse strain with rapidly progressive glomerulonephritis and small vessel vasculitis. *Proc Natl Acad Sci USA* 1993; 90: 3413–3417
18. Miyazawa S, Saiga K, Nemoto K *et al.* A repeat biopsy study in spontaneous crescentic glomerulonephritis mice. *Ren Fail* 2002; 24: 557–566
19. Dewas C, Dang PM, Gougerot-Pocidalo MA *et al.* TNF-alpha induces phosphorylation of $p47^{phox}$ in human neutrophils: partial phosphorylation of $p47^{phox}$ is a common event of priming of human neutrophils by TNF-alpha and granulocyte-macrophage colony-stimulating factor. *J Immunol* 2003; 171: 4392–4398
20. Timoshanko JR, Sedgwick JD, Holdsworth SR *et al.* Intrinsic renal cells are the major source of tumor necrosis factor contributing to renal injury in murine crescentic glomerulonephritis. *J Am Soc Nephrol* 2003; 14: 1785–1793
21. Bajema IM, Hagen EC, de Heer E *et al.* Colocalization of ANCA-antigens and fibrinoid necrosis in ANCA-associated vasculitis. *Kidney Int* 2001; 60: 2025–2030
22. Potter PK, Cortes-Hernandez J, Quartier P *et al.* Lupus-prone mice have an abnormal response to thioglycolate and an impaired clearance of apoptotic cells. *J Immunol* 2003; 170: 3223–3232

Received for publication: 10.6.03
Accepted in revised form: 14.1.04

Available online at www.sciencedirect.com
SCIENCE DIRECT®
Gene 327 (2004) 195–200
GENE
AN INTERNATIONAL JOURNAL ON GENES AND GENOMES
www.elsevier.com/locate/gene

Novel missense mutation found in a Japanese patient with myeloperoxidase deficiency

Yuko Y. Ohashi[a], Yosuke Kameoka[b], Amanda S. Persad[a], Fumikazu Koi[c], Satoshi Yamagoe[a], Katsuyuki Hashimoto[b], Kazuo Suzuki[a,*]

[a] *Department of Bioactive Molecules, National Institute of Infectious Diseases, 1-23-1 Toyama, Shinjuku, Tokyo 162-8640, Japan*
[b] *Division of Genetic Resources, National Institute of Infectious Diseases, 1-23-1 Toyama, Shinjuku, Tokyo 162-8640, Japan*
[c] *Takamatsu Kyosai Hospital, 4-18 Tenjinmae, Takamatsu City 760-0081, Japan*

Received 23 July 2003; received in revised form 5 November 2003; accepted 14 November 2003

Abstract

Myeloperoxidase (MPO; EC 1.11.1.7) plays an important role in the host defense mechanism against microbial diseases. The neutrophil disorder characterized by the lack of MPO activity, is speculated to be associated with a decreased level of immunity. A Japanese patient was identified with complete MPO deficiency through automated hematography. Neutrophil function analysis revealed that MPO activity was significantly diminished with slightly elevated superoxide production. Mutational analysis of the patient revealed a glycine to serine substitution (G501S) in the exon 9 region. This mutation was not detected in the 96 healthy controls analyzed. The amino acid substitution found may be responsible for the failure of mature MPO production in the patient. This is the first case of MPO deficiency of G501S missense mutation identified in a Japanese patient.

Keywords: Myeloperoxidase; Deficiency; Neutrophills; Mutation heme-binding

1. Introduction

Myeloperoxidase (MPO) is a lysosomal heme protein located in azurophilic granules of neutrophils cells and monocytes. MPO is part of the host defense system and is responsible for microbicidal activity against a wide range of organisms. In activated neutrophils, MPO catalyzes the production of hypohalous acids, primarily hypochlorous acid and other toxic intermediates that greatly enhance neutrophil microbicidal activity. A deficiency in this enzyme (Mendelian inheritance in man (MIM) no. 254600) is considered to be responsible for weakening host defense activity against microbial diseases (Lanza, 1998). The prevalence of complete MPO deficiency in Japan is estimated to be 1.75/100,000, a value 14- to 28-fold lower than that of the United States and Europe, respectively (Suzuki et al., 2000; Nunoi et al., 2003). Aratani et al. (1999, 2000) has described the association with this deficiency and continuous infection of *Candida albicans* in MPO knock-out mice.

Three allelic mutations related to MPO deficiency have been previously reported: R569W (Nauseef et al., 1994, 1996), Y173C (DeLeo et al., 1998) and M251T (Romano et al., 1997). The defect mechanisms and manner of inheritance has been studied in detail (Nauseef et al., 1996, 1998). The enzyme deficiency is due to incapability to undergo posttranslational processing. Cases with alternative splicing and deletions have also been reported (Romano et al., 1997; Hashinaka et al., 1988).The biosynthesis of MPO includes N-linked glycosylation, heme insertion, proteolytic processing and dimerization (Gullberg et al., 1997). The R569W mutation results in an alteration in the normal translation and produces an enzymatically inactive, heme-free precursor apoproMPO (Nauseef et al., 1996). The Y173C mutation replaces the tyrosine at position 7 in the light subunit

Abbreviations: MPO, myeloperoxidase; BGL, beta-glucuronidase; HBSS, Hanks' balance salt solution; PVDF, polyvinylidene difluoride; AP, alkaline phosphatase; cDNA, DNA complementary to RNA; PCR, polymerase chain reaction; RT, reverse transcriptase; mRNA, messenger RNA; RT–PCR, polymerase chain reaction subsequent to reverse transcription.

* Corresponding author. Tel.: +81-3-5285-1111x2329; fax: +81-3-5285-1160.
E-mail address: ksuzuki@nih.go.jp (K. Suzuki).

0378-1119/$ - see front matter © 2004 Elsevier B.V. All rights reserved.
doi:10.1016/j.gene.2003.11.023

with a cysteine. Therefore, the potential for additional intramolecular disulfide bond would be created. Y173C mutation results in proMPO, however, it fails to mature into the enzymatically active MPO (DeLeo et al., 1998). The M251T mutation results in azurophilic granules, containing MPO that lacks enzyme activity (Romano et al., 1997).

We have found a patient of complete MPO deficiency in Japan. So far, no MPO mutational study among Japanese patients has been reported. In order to elucidate the background of the deficiency, we performed assays for enzyme activity and neutrophil chemotaxis, as well as mutational analysis of the patient and his mother.

2. Materials and methods

2.1. Subjects

A 39-year-old Japanese male was diagnosed with complete MPO deficiency by Bayer-Technicon automated hematography (Suzuki et al., 2000). Automated hematography is routinely used in the hospital system to further analyze unusual neutrophil activity. Informed consent was obtained from the patient and his mother (60 years old) for this study. The patient exhibited signs of obstructive pulmonary disease, although no history of recurrent infections or medication known to interfere with MPO activity were present or used. A blood sample from one healthy control was drawn to measure enzyme activity and superoxide production, however, controls for genetic sequencing consisted of DNA samples from 98 healthy donors of which MPO activity and superoxide activity could not be elucidated. Since MPO deficiency (both complete and partial deficiency) is very rare in Japan, less than 6 cases per 100,000 individuals, it is highly unlikely that these 98 healthy donors were deficient in this enzyme (Suzuki et al., 2000; Nunoi et al., 2003).

2.2. Assay of MPO release from neutrophils

MPO release from neutrophils was assayed as described previously (Kawai et al., 2000). Neutrophils (10^6 cells/ml in Hanks' balance salt solution, HBSS) were prewarmed for 10 min at 37 °C and transferred into a 96-well V-plate containing cytochalasin B (CB; 5 μg/ml) (Sigma-Aldrich Japan, Tokyo) and fMet–Leu–Phe (FMLP, 10^{-5} M) (Protein Research Foundation, Osaka) in a total volume of 75 μl. After incubation for 10 min at 37 °C, cell suspensions were centrifuged at $400 \times g$ for 5 min. MPO activity in the supernatant and in the homogenate of the cell pellet was measured spectrophotometrically using 3,3′, 5,5′-tetramethylbenzidine as substrate (Suzuki et al., 1983, 1986). The total enzyme activity of MPO in neutrophils was calculated as the sum of enzyme activity in supernatants and homogenate after treatment with CB and FMLP. Release of MPO was expressed as percentage of total enzyme activity (MPO activity in supernatant/total enzyme activity).

2.3. Measurement of beta-glucuronidase (BGL) activity

Beta-glucuronidase activity and release was elicited by methods described previously (Minoshima et al., 1997). Cell supernatant and homogenate (40 μl) was treated with 1 mmol/l 4-methylumbelliferyl-beta-D-glucuronide, 0.05% Triton X-100 and 0.1 mol/l sodium acetate buffer (pH 3.5) in 96-well flat bottom plate. After 30 min of incubation at 37 °C, the reaction was stopped by adding 210 μl of termination buffer (50 mmol/l sodium glycine buffer pH 10.4 supplemented with 5 mmol/l EDTA). Fluorescence intensity was measured by using an automated fluorescence analyzer LFA-096F (Japan Spectroscopic, Tokyo, Japan). One unit of BGL activity was defined as the activity of 1 pmol of 4-methylumbelliferon/min per milliliter of the original enzyme preparation.

2.4. Determination of O_2^- production by neutrophils

Superoxide (O_2^-) production by neutrophils was determined using methods previously described (Kawai et al., 2000). Briefly, neutrophil suspensions (2.0×10^6 cells/ml, 100 μl) and 66 μM of ferricytochrome *c* (Sigma-Aldrich Japan) were mixed in a 96-well F-plate and held at 37 °C for approximately 2 min. CB (5 μg/ml) and FMLP (10^{-5} M) were added to the suspension and incubated for approximately 30 s at 37 °C. An initial velocity of O_2^- production was determined by measuring the increase in absorbance at 550 nm at 1.0-min intervals using a microplate reader.

2.5. Western blot analysis

Immunoblotting of neutrophils from patient, his mother and healthy control was performed as follows. The neutrophils (2×10^6 cells/200 μl) and purified MPO (100 ng/10 μl) were dissolved in loading buffer (50 mM Tris–HCl pH6.8, 10% glycerol, 1% SDS, 0.3 M beta-mercaptoethanol, 0.01% BPB) and incubate for 5 min at 98 °C to ensure completed reduction conditions, then quickly chilled on ice. Ten milliliters of each sample was fractionated on an 8–12% SDS–polyacrylamide gel according to Laemmli's system (Laemmli, 1970) and electrically transferred on to a polyvinylidene diflouride (PVDF) membrane (Millipore, Bedford, MA) in transfer buffer (20% methanol, 25 mmol/l Tris, 0.19 mol/l glycine). Membrane was incubated with a 1:2000 anti-human MPO rabbit antibody (Dako, Glostrup, Denmark) at room temperature for 2 h, followed by an incubation with a 1:2000 alkaline phosphatase (AP)-conjugated anti-rabbit IgG goat antibody (Organon Teknika, Durham, NC) for 2 h. Finally, the membrane was visualized using AP conjugate substrate kit (Bio-Rad, Hercules, CA, USA).

2.6. cDNA and genomic DNA analysis

MPO cDNA was acquired from the mRNA of mononuclear cells (MNC) by polymerase chain reaction (PCR)

Table 1
PCR primers used to detect (a) mRNA and (b) genomic sequence of MPO

DNA fragment	F/R	Position	Sequence (5′–3′)
(a) mRNA			
Fragment 1	F	−148	ccttggaagctggatgacagcagct
	R	+346	gctgactacctgcacgtggct
Fragment 2	F	+295	ctatcctacttcaagcagccg
	R	+741	cgctcactcatgttcatgcaa
Fragment 3	F	+694	aacgagatcgtgcgcttcccc
	R	+1123	ggcctgctgccctttgacaac
Fragment 4	F	+1063	aacatgtccaaccagctgggg
	R	+1530	aatcggtaccagcccatggaa
Fragment 5	F	+1498	tacggccacaccctcatccaa
	R	+1960	aaaggccgcgtgggcccactc
Fragment 6	F	+1918	atcgacatctggatgggcggc
	R	+2406	ggcttttcatgcgtgaaaaaaa
(b) Genomic fragment			
5′-flanking	F	−556	ctgagaaatcttgggctggtagtgct
	R	+36	tccttggaagctggatgacagcagct
Exon 1	F	−66	agaggacataaaagcgcag
	R	+302	aaggtgggagaagatggtgt
Exon 9	F	+7195	agatacttcccctgacctgg
	R	+7495	gacctaggccagagcgagtg

Primers were designed from the published sequence (Genbank accession nos. X04876 and X15377).
F = forward primer; R = reverse primer. Positons of primer are indicated by base number from the adenine of the first ATG.

using the One Step RNA PCR Kit (Takara, Kyoto, Japan). The specific primer pairs for MPO mRNA are shown in Table 1. DNA segments obtained were purified by the QIAquick PCR purification system (Qiagen, Hilden, Germany) and subjected to direct sequencing as described by the manufacturer. Purified fragments served as templates in a PRISM Ready Reaction Dye Terminator Cycle Sequencing procedure utilizing a 310 automatic sequencer (Applied Biosystems, Foster City, CA, USA). Primers used for sequencing are listed in Table 1. Additionally, the prevalence of −463 G/A polymorphism, a previously described mutation found in the promoter region of MPO (Reynolds et al., 2002), among controls was ascertained.

3. Results

3.1. Neutrophil functions and MPO activity

Total MPO activity of the patient was 250-fold lower than the healthy control, while the mother had half the activity of the control (Table 2). FMLP and cytochalasin B-induced MPO release was not detected in the patient, while the released MPO activity of the mother and the healthy control showed no marked difference. To examine the normal formation of azurophil granules, in which MPO is enclosed, BGL release and O_2^- production were assayed. BGL release was elicited by methods described previously (Minoshima et al., 1997). The patient, patient's mother and healthy control showed no difference in BGL and O_2^- production.

Table 2
Enzyme activities and functions of polymorphonuclear cells

	MPO		BGL		O_2^- production (nmol/min/10^6 cells)
	Total activity unit	% Release	Total activity unit	% Release	
Patient	0.3	N.D.	570	55.2	18
Mother	30.5	33.5	651	24.1	10.9
Healthy control	75.7*	22.9	430	32.7	14.1

N.D. = not detected; N.T. = not tested.
* Average in two experiments.

Azurophil granule formation under histochemical observation and O_2^- production of the patient showed no substantial difference from healthy control. Neutrophils may have developed normally but lack only mature MPO protein. As the mother showed half the MPO activity of the healthy control, there might be a quantitative effect of an abnormal allele in the mother.

3.2. Western blot analysis

In order to biochemically characterized MPO, immunoblotting analysis of the neutrophils from the healthy control, the patient, his mother and purified MPO were performed using anti-human MPO antibody. As shown in Fig. 1, the 59-kDa mature heavy subunit and the 14-kDa light subunit could not be detected in the patient, while the healthy control and mother had both mature subunits.

3.3. Mutational analysis

MPO cDNA, acquired by reverse transcription (RT)–PCR, were found to be the appropriate length in for each fragment amplified. Therefore, MPO gene in the patient was normally transcribed without any alternative transcription.

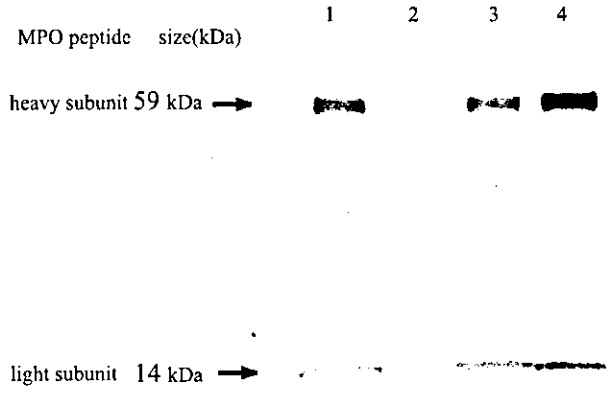

Fig. 1. Western blot analysis. Proteins in neutrophils (1×10^5 cells/lane) of healthy control, the patient, his mother and purified MPO protein (100 ng/lane) was fractionated on 8–12% polyacrylamide gel, transferred on PVDF membrane, and detected by rabbit anti-human MPO antibody. Lane 1, healthy control; lane 2, patient; lane 3, mother; and lane 4, purified human MPO. MPO polypeptides were indicated in the left.

The RT–PCR products obtained were directly sequenced and compared with a normal MPO cDNA sequence (Johnson et al., 1987; Morishita et al., 1987; Yamada et al., 1987). A guanine (G) to adenine (A) substitution was found in exon 9 region of the patient cDNA. This point mutation was located at position 1051 from adenine of first ATG (Fig. 2) and resulted in an amino acid conversion from glycine (GGC) to serine (AGC), G501S.

Genomic DNA for the MPO coding region and 5′ promoter region of the patient and his mother were amplified and sequenced to confirm the base substitution of the allele. The G to A substitution in exon 9 shown in Fig. 2b, was homozygous in the patient, but heterozygous in the patient's mother. This same exon was successfully sequenced and analyzed in 96 genomic DNA samples from healthy Japanese controls; sequencing for two of the original 98 controls was unsuccessful. None of these samples exhibited the G1051A mutation (Table 3). Analysis of the 5′ promoter region (− 463 from the first ATG), a polymorphic site, of patient, his mother and simultaneously prepared control samples revealed a homozygous guanine at that site (data not shown).

Table 3
Base substitutions of MPO gene

Source	Position of base substitution	
	5′ flanking region	Exon 9
	− 463	1051
Referred nucleotide*	A	G
Patient	G/G	A/A
Mother	G/G	A/G
Healthy control	G/G	G/G
Controls (N=96)	83% G/G 15% G/A 1% A/A	100% G/G

*Nucleotides from Genbank accession nos. X04876 and X15377.

4. Discussion

A single base substitution has been identified in the MPO cDNA in a patient with complete MPO deficiency. This G1051A mutation resulted in an amino acid change (G501S), which may have resulted in the said deficiency of the patient (Fig. 3). We could not detected mature MPO subunits (heavy and light subunit), although by Western blot analysis, we could detect 90-kDa prepro-MPO, which is the precursor of mature MPO subunits. The MPO mRNA from the patient did not reveal any alternative splicing sites and deletions. The − 463 G/A polymorphic site did not appear to play a role in this MPO deficiency, since there was no base difference between the patient and the 96 controls. Additionally, the allele frequency among the controls complied with data previously reported in the Japanese population with a predominance of the G/G genotype at that site (Hamajima et al., 2002) (Table 3).

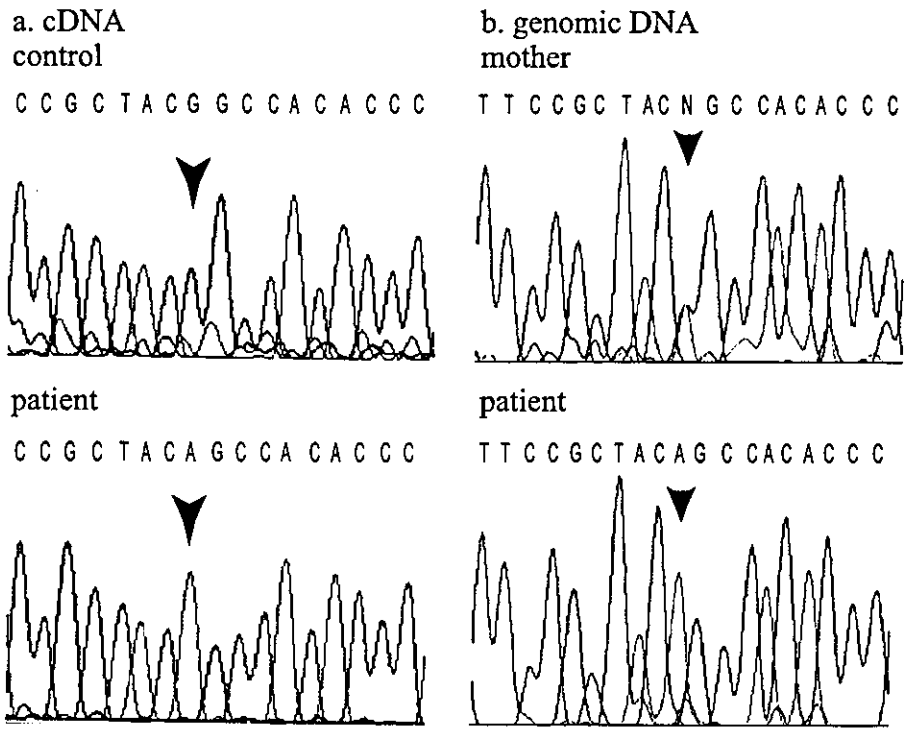

Fig. 2. Sequence histogram around the mutation point of cDNA and genomic DNA. (a) cDNA sequence of the patient and healthy control. The mutation position of 1051 was indicated with arrow heads. (b) Same coding region in genomic DNA of the patient and his mother.

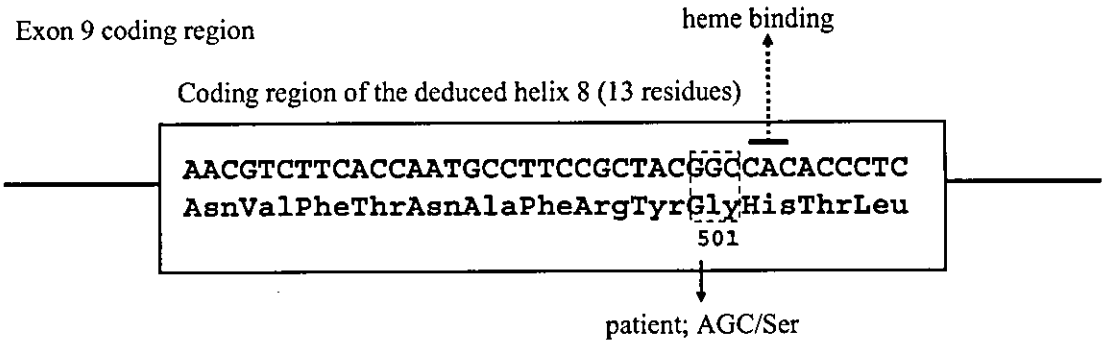

Fig. 3. Schematic diagram of exon 9. Amino acid residues and base sequence of deduced helix 8 region was shown in the box. G1051A causes amino acid substitution glysine to serine. His502 is a heme binding residue.

Three missense mutations on MPO gene which causes MPO deficiency, R569W (Nauseef et al., 1994, 1996), Y173C (DeLeo et al., 1998) and M251T (Romano et al., 1997) have been reported. Mature subunits of the enzyme are not formed in cases with R569W and Y173C mutation because posttranslational processing cannot be carried out correctly. M251T causes mature subunit but lacks enzymatic activity. The histidine at codon 502 (H502), which is included in the eighth helix domain constituting one part of heme-binding pocket, provides proximal ligand to the heme iron (Zeng and Fenna, 1992; Davey and Fenna, 1996). The missense mutation G501S is located adjacent to H502, also included in the eighth helix. The glycine to serine substitution possibly influenced the surrounding molecular environment of amino acid residues, especially the neighboring histidine residue, which plays an important role in heme binding. Thus, the G501S could cause an arrest in heme binding, an essential step for maturation of the enzymatically active MPO.

References

Aratani, Y., Koyama, H., Nyui, S., Suzuki, K., Kura, F., Maeda, N., 1999. Severe impairment in early host defense against *Candida albicans* in mice deficient in myeloperoxidase. Infect. Immun. 67, 1828–1836.

Aratani, Y., Kura, F., Watanabe, H., Akagawa, H., Takano, Y., Suzuki, K., Maeda, N., Koyama, H., 2000. Differential host susceptibility to pulmonary infections with bacteria and fungi in mice deficient in myeloperoxidase. J. Infect. Dis. 182, 1276–1279.

Davey, C.A., Fenna, R.E., 1996. 2.3 A resolution X-ray crystal structure of the bisubstrate analogue inhibitor salicylhydroxamic acid bound to human myeloperoxidase: a model for a prereaction complex with hydrogen peroxide. Biochemistry 20;35 (33), 10967–10973.

DeLeo, F.R., Goedken, M., McCormick, S.J., Nauseef, W.M., 1998. A novel form of hereditary myeloperoxidase deficiency linked to endoplasmic reticulum/proteasome degradation. J. Clin. Invest. 101, 2900–2909.

Gullberg, U., Andersson, E., Garwicz, D., Lindmark, A., Olsson, I., 1997. Biosynthesis, processing and sorting of neutrophil proteins: insight into neutrophil granule development. Eur. J. Haematol. 58, 137–153.

Hamajima, N., Saito, T., Matsuo, K., Suzuki, T., Nakamura, T., Matsuura, A., Okuma, K., Tajima, K., 2002. Genotype frequencies of, 50, polymorphisms for, 241 Japanese non-cancer patients. J. Epidemiol. 12, 229–236.

Hashinaka, K., Nishio, C., Hur, S.J., Sakiyama, F., Tsunasawa, S., Yamada, M., 1988. Multiple species of myeloperoxidase messenger RNAs produced by alternative splicing and differential polyadenylation. Biochemistry 27, 5906–5914.

Johnson, K.R., Nauseef, W.M., Care, A., Wheelock, M.J., Shane, S., Hudson, S., Koeffler, H.P., Selsted, M., Miller, C., Rovera, G., 1987. Characterization of cDNA clones for human myeloperoxidase: predicted amino acid sequence and evidence for multiple mRNA species. Nucleic Acids Res. 15, 2013–2028.

Kawai, Y., Okawarab, A.I., Okuyama, H., Kura, F., 2000. Modulation of chemotaxis, O2-production and myeloperoxidase release from human polymorphonuclear leukocytes by the ornithine-containing lipid and serineglycine-containing lipid of *Flavobacterium*. FEMS Immunol. Med. Microbiol. 28, 205–209.

Laemmli, U.K., 1970. Cleavage of structural proteins during the assembly of the head of bacteriophage T4. Nature 15;227 (259), 680–685.

Lanza, F., 1998. Clinical manifestation of myeloperoxidase deficiency. J. Mol. Med. 76, 676–681.

Minoshima, S., Arimura, Y., Nakabayashi, K., Kitamoto, K., Nagasawa, T., Okawara, A.I., Suzuki, K., 1997. Increased release of myeloperoxidase in vitro from neutrophils of patients with myeloperoxidase-specific antineutrophil cytoplasmic antibody (MPO-ANCA) related glomerulonephritis. Nephrology 3, 527–534.

Morishita, K., Kubota, N., Asano, S., Kaziro, Y., Nagata, S., 1987. Molecular cloning and characterization of cDNA for human myeloperoxidase. J. Biol. Chem. 262, 3844–3851.

Nauseef, W.M., Brigham, S., Cogley, M., 1994. Hereditary myeloperoxidase deficiency due to a missense mutation of arginine, 569, to tryptophan. J. Biol. Chem. 269, 1212–1216.

Nauseef, W.M., Cogley, M., McCormick, S., 1996. Effect of the R569W missense mutation on the biosynthesis of myeloperoxidase. J. Biol. Chem. 271, 9546–9549.

Nauseef, W.M., Cogley, M., Bock, S., Petrides, P.E., 1998. Pattern of inheritance in hereditary myeloperoxidase deficiency associated with the R569W missense mutation. J. Leukoc. Biol. 63, 264–269.

Nunoi, H., Kohi, F., Kajiwara, H., Suzuki, K., 2003. Prevalence of inherited myeloperoxidase deficiency in Japan. Microbiol. Immunol. 47, 527–531.

Reynolds, W.F., Stegeman, C.A., Cohen Tervaert, J.W., 2002. −463 G/A Myeloperoxidase promoter polymorphism is associated with clinical manifestations and the course of disease in MPO-ANCA-associated vasculitis. Clin. Immunol. 103, 154–160.

Romano, M., Dri, P., Dadalt, L., Patriarca, P., Baralle, F.E., 1997. Biochemical and molecular characterization of hereditary myeloproliferative deficiency. Blood 90, 4126–4134.

Suzuki, K., Ota, H., Sasagawa, S., Sakatani, T., Fujikura, T., 1983. Assay method for myeloperoxidase in human polymorphonuclear leukocytes. Anal. Biochem. 132, 345–352.

Suzuki, K., Yamada, M., Akashi, K., Fujikura, T., 1986. Similarity of kinetics of three types of myeloperoxidase from human leukocytes

and four types from HL-60 cells. Arch. Biochem. Biophys. 245, 167–173.

Suzuki, K., Nunoi, H., Miyazaki, M., Koi, F., 2000. Prevalence of inherited myeloperoxidase deficiency in Japan. In: Petrides, P.E., Nauseef, W.M. (Eds.), The Peroxidase Multigene Family of Enzymes. Springer-Verlag, Berlin, pp. 145–149.

Yamada, M., Hur, S.J., Hashinaka, K., Tsuneoka, K., Saeki, T., Nishio, C., Sakiyama, F., Tsunasawa, S., 1987. Isolation and characterization of a cDNA coding for human myeloperoxidase. Arch. Biochem. Biophys. 255, 147–155.

Zeng, J., Fenna, R.E., 1992. X-ray crystal structure of canine myeloperoxidase at 3 A resolution. J. Mol. Biol. 226, 185–207.

Available online at www.sciencedirect.com
SCIENCE DIRECT®
Biochemical and Biophysical Research Communications 314 (2004) 46–53
BBRC
www.elsevier.com/locate/ybbrc

Applications of T-lymphoma labeled with fluorescent quantum dots to cell tracing markers in mouse body

Akiyoshi Hoshino,[a,b] Ken-ichi Hanaki,[a] Kazuo Suzuki,[b] and Kenji Yamamoto[a,*]

[a] *Department of Medical Ecology and Informatics, Research Institute, International Medical Center of Japan, 1-21-1 Toyama, Shinjuku, Tokyo 162-8655, Japan*
[b] *Department of Bioactive Molecules, National Institute of Infectious Diseases, 1-23-1 Toyama, Shinjuku, Tokyo 162-8640, Japan*

Received 25 November 2003

Abstract

Photoluminescent semiconductor quantum dots (QDs) are novel nanometer-size probes that have found bioimaging. Here we imaged a cell line of mouse lymphocytes. QDs were actively taken into the target cells by endocytotic pathways. The fluorescence of QDs held in the endosomes could be studied for more than a week and remained stable luminescence against cell activation induced by concanavalin A, phytohemagglutinin, phorbol myristate acetate, and calcium ionophore A23187. These results suggested that QD-labeling was stable and did not affect either cell activation or cell function. When QD-labeled cells were intravenously injected into mouse, they remained in the peripheral blood in a concentration of approximately 10% up to 5 days after injection using both fluorescence microscopy and flow cytometry. In addition, approximately 20% of QDs were detected in the kidneys, liver, lung, and spleen and could still be observed 7 days after injection. These results suggested that fluorescent probes of QDs might be useful as bioimaging tools for tracing target cells over the period of a week in vivo.

Keywords: Bioimaging; Cell labeling marker; Cytotoxicity; In vivo; Living cell; Quantum dot; Semiconductor

Ultrafine nanocrystals are expected to be used widely in biotechnology and medical applications for separating biomaterials, immunoassay, diagnostics, and drug-carriers that are applied to the drug delivery systems [1–6]. Quantum dots (QDs) are novel inorganic fluorophores that consist of CdSe/ZnS-core/shell semiconductor nanocrystals. QDs have several advantages over organic fluorophores. QDs show high luminance, resistance to photobleaching, a range of excitement wavelengths from ultraviolet to red that depend on the size of the particles, and cover a range of fluorescent wavelengths from blue to red that can be excited using a mercury arc lamp [7,8]. At present, many organic fluorophores such as fluorescein isothiocyanate (FITC) and carboxyfluorescein diacetate succinimidyl ester (CFSE) have been used in various biological applications, such as fluorescent-labeled antibodies and molecules that are used to stain cells or cellar organs [8,9]. Experiments using organic dyes are limited to short-time assays such as flow cytometry due to the lifetime of fluorescence. Those dyes were not suitable for extended periods of bioimaging observations using fluorescent and confocal microscopy because organic fluorophores tend to quench rapidly [6,10]. Furthermore, it is sometimes difficult or impossible to record fine fluorescent images while the organic coloring probes fade in the course of adjusting the focus. In contrast, QDs are stabilized over a far longer exposure-time to light and can emit a fluorescence of high luminosity at an almost equivalent condition as the conventional organic fluorescence probes.

Initially, chemically synthesized QDs have not been applied to biochemical applications because they do not dissolve in water. Since hydrophilic surface treatment of QD was developed, the application range of QDs has been rapidly spreading to bioimaging [11–13]. However, QDs can easily aggregate at acidic- and even in isotonic-conditions because they are unstable in either acidic or saline conditions. Hence, QD-conjugated biomolecules are difficult to produce because most of the biomolecules

* Corresponding author. Fax: +81-3-3202-7364.
E-mail address: backen@ri.imcj.go.jp (K. Yamamoto).

0006-291X/$ - see front matter © 2003 Elsevier Inc. All rights reserved.
doi:10.1016/j.bbrc.2003.11.185

exist in the isotonic condition in vivo [14]. The molecules that can conjugate with QDs are few: streptavidin, oligopeptides, and some antibodies [13,15,16]. We have considered methods to stabilize QDs in biological solutions such as culture media [11,17]. We previously examined albumin from 10 species to assess efficient stabilization since QDs could be conjugated to albumin non-specifically [17]. Time-lapse study of the intracellular distribution of QDs in culture cells has already been performed and the endosomal vesicles including QDs were observed [17]. In this study we assessed whether QDs could be applied to various applications using labeled cells for the purpose of long-time tracing. Labeled concentration of QDs did not appear to show any signs of cytotoxicity. Although there are many applications where QDs are used as dyes to stain mammalian cells and bacteria in vitro [17,18], no applications have been demonstrated where QDs can be used in cells that are transplanted into the living animals.

Materials and methods

Reagents and preparation of albumin-conjugated QDs. CdSe/ZnS-core/shell QDs (fluorescence wavelength: 520 nm) were conjugated with sheep serum albumin fraction V (Sigma) according to our study, as previously reported [17]. Briefly, albumin-conjugated QDs were prepared by mixing equal volumes of QD-sodium salt solution (10 mg/ml) and sheep albumin solution (10 mg/ml) in the presence of EDC (1-ethyl-3-[3-dimethylaminopropyl]carbodiimide hydrochloride) coupling reagents purchased from Pierce Biochemical. The mixture was incubated for 30 min at room temperature and applied to a Sephadex G-25 column (Amersham Biosciences) to remove the excess fraction of reagents. The QD-working solution was prepared by diluting the QD-mixture with DMEM/F-12 culture media (Gibco), immediately filtered with a 0.1-μm centrifuge membrane filter (Millipore, Ultrafree-MC), and centrifuged at 10,000*g* for 10 min before use.

Assessment of QD-Uptake by cells. EL-4 cells, which were established from murine T-cell lymphoma, were cultured in DMEM/F12 supplemented with 5% heat-inactivated fetal bovine serum at 37 °C. The cells were plated at a volume of 1×10^6 cells/well on a 12-well culture plate (Iwaki) and were stimulated with the indicated concentration of QDs. After incubation, the cells were harvested and washed with phosphate-buffered saline (PBS) twice to remove the non-specific binding QDs. The cells were stained with 100 μg/ml propidium iodide solution. Then the cells were fixed with 10%-formaldehyde neutral buffer. As many as 1×10^6 cells were analyzed by flow cytometer (JASCO CytoAce300). Fluorescence was excited using argon laser (488 nm). Detection was triggered by forward-angle light-scattered signals at wavelength of 520 nm. Images were acquired with a digital camera D1X (Nikon) on a fluorescent microscope IX-81 (Olympus) using WIBA mirror unit to adjust the excitation wavelength to 470–490 nm and oil immersion objective lens.

Mice and separation of the cells and organ. BALB/c AnNCrj-nu/nu (nude) mice (5w, male) were purchased from Charles River Japan Inc. EL-4 cells used for administration were pre-stained with a PKH26 Red Fluorescent Cell Linker Kit purchased from Sigma before stimulation with albumin-conjugated QDs. The cells holding QDs were collected 2 h after stimulation and resuspended to the concentration of 5×10^7 cells/ml in serum-free DMEM/F12. Two hundred microliters of cell-suspended solution was intravenously injected to mice. The mice were sacrificed 2 h, 1 day, 3 days, 5 days, and 7 days after injection and the peripheral blood was collected. The blood was laid onto a Ficoll–Metrizoate density gradient (Histopaque-1083 solution, Sigma) and centrifuged at 700*g* for 30 min at room temperature to form a distinct layer at the plasma-media interface. The leukocyte fraction including EL-4 cells was separated from the interface of the two solutions. Then contaminated erythrocytes were removed by 2 washes in ACK-lysis buffer (150 mM NH_4Cl, 1 mM $KHCO_3$, and 0.1 mM EDTA, pH 7.4). Each lysis was performed by incubating for 5 min at room temperature followed by washing the cells with PBS twice. Fluorescence intensity of QD-holding cells was detected by flow cytometric analysis and by fluorescent microscopy.

Collected kidney, liver, lung, and spleen organs were immediately washed three times by PBS to remove retained erythrocytes. Then each organ was incubated with 4% paraformaldehyde for 2 h at room temperature. After soaking, the organs were washed and incubated with 70% ethanol at 4 °C overnight. After embedding into paraffin, the section was sliced to 10 μm thickness. The section was affixed to slide glass (Matsunami).

Results and discussion

Many researchers have applied various techniques to recognize the introduced target cells specifically; labeled cells directly with organic fluorophores like CFSE [8,9], dyed X–Y chromosome by fluorescence in situ hybridization (FISH) using sex-mismatched target cells [19], transformed the gene coded specific molecule like green fluorescent proteins (GFPs), various kind of luciferases, or some cell surface expression molecules, etc. [20,21]. But unfortunately, it gets hanged up and it is costly to detect the target cells by these procedures. To remove those problems, we assessed the possibility of using QDs as the markers for the introduced target cells in vivo. First, we examined how long it took for the EL-4 cells to take up the albumin-conjugated QDs. EL-4 cells were plated at 1×10^6 cells/well and stimulated with 0.1 mg/ml QDs for 15, 30, and 60 min at 37 °C. Shown in Fig. 1A, the QDs were adherent to the cell surface 15 min after incubation. The vesicles including QDs started to form 30 min after incubation and QDs were recruited into the cellular granules after 60 min. We assumed that this uptake would be inhibited at chilled conditions if it were performed via endocytotic pathways. To investigate whether this uptake reaction was dependent on their temperature, EL-4 cells were cultured with QDs at chilled condition. As expected, QDs were also found adhering to the cell surface, but uptake into the cell vesicles was blocked even after 60 min incubation (Fig. 1A). In addition, re-incubating the cells at 37 °C, the QD uptake into the cells recovered again (Fig. 1B). This adhesion is not detached by washing the QD-holding cells and fluorescence of the cells was measured by flow cytometry, which was the same as at 37 °C conditions. These results suggested that uptake of QDs into the cells occurs via endocytotic pathways. This indicated that processing for 15 min to stain the cell surface is sufficient for the purpose of short-time cell tracing. Thus, QDs can become an effective cell marker for several days after only short-time treatment of the cell.

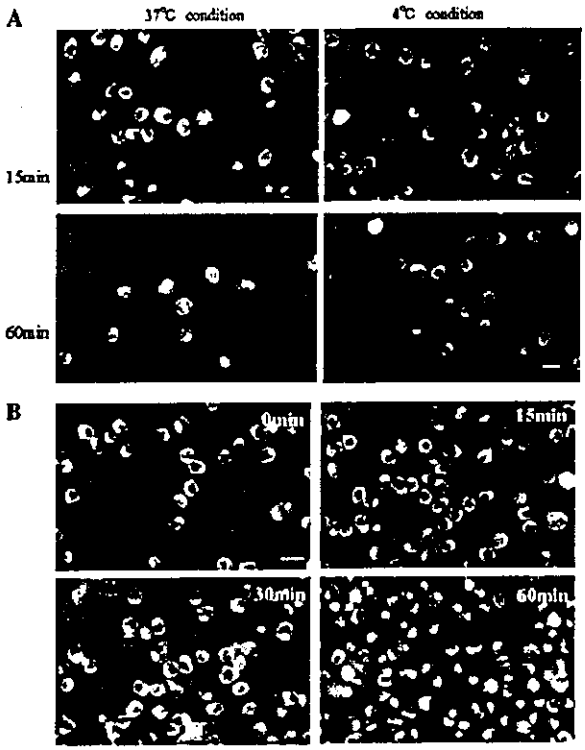

Fig. 1. Uptake of albumin-conjugated QD by EL-4 cells was dependent on temperature. (A) EL-4 murine lymphocytoma cells were plated and stimulated with albumin-conjugated QD at the concentration of 0.1 mg/ml and incubated for 15 and 60 min at 37 and 4 °C conditions. QD- labeled cells were observed by fluorescent microscopy. The bright green granules indicated fluorescence emitted from QDs. (B) Cells were pre-incubated for 20 min before stimulation. Then the cells were stimulated with QDs for 60 min at 4 °C condition and re-incubated at 37 °C for the indicated time. Bars indicate 10 μm. In all the figures, the observation data represent one out of three performed.

When QDs were used as long-term tracing markers, the acute cytotoxicity of QDs raises a problem. To investigate the relation between concentration and cytotoxicity of QDs, we assessed the cell viability after QD-stimulation. The cells were cultured at the concentration of 0.1, 0.2, and 0.4 mg/ml of QDs for 24 h and stained with propidium iodide to detect dead cells. As the fluorescence intensity of QD-holding cells increased by the concentration of QDs, the number of dead cells also increased (Fig. 2). The cytotoxicity was observed in proportion to the concentration of QDs and almost all of the cells were dead at 0.4 mg/ml more than 6 h after incubation. However, no remarkable cytotoxicity was observed at 0.1 mg/ml. Since using a high-concentration of QDs induced the cell death, we decided to use QDs at 0.1 mg/ml concentration.

Next we also examined how long QDs could be retained in the cells. To investigate this, EL-4 cells were further cultured after stimulation with QDs. Cell growth of EL-4 cells was choked by stimulation with QDs even

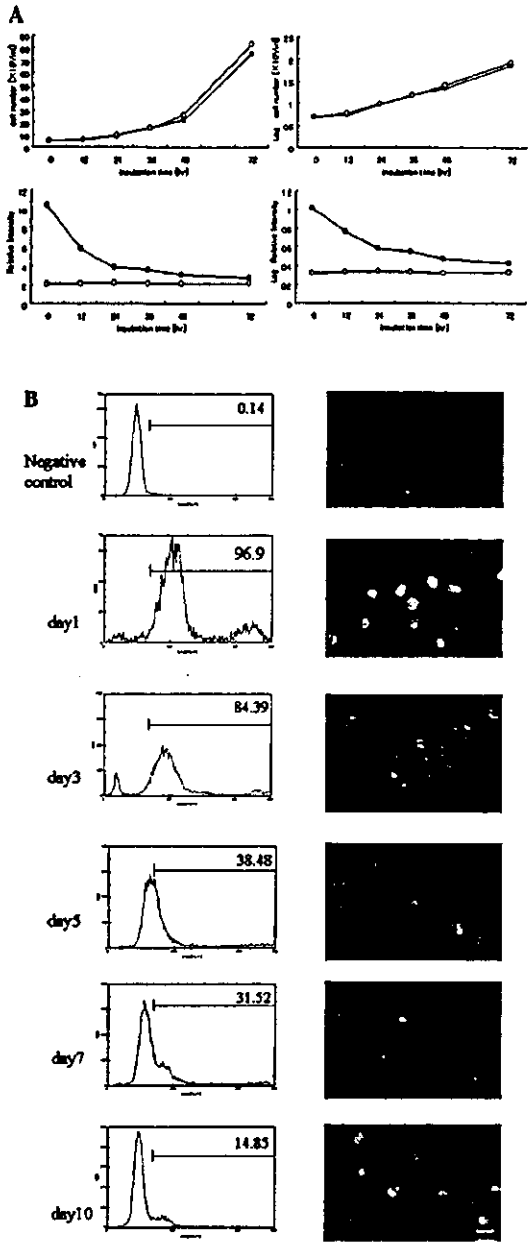

Fig. 3. QDs labeled on EL-4 cells were observed more than a week in vitro. (A) The *upper graphs* show a comparison between the growth curve of the unlabeled and QD-labeled EL-4 cells; open circles indicated the number of control cells and the closed circles are the QDs, respectively. The *lower graphs* show the relative fluorescence intensity of 10^5-collected cells measured by spectrofluorometer (JASCO, FP-6500); open circles indicated the fluorescence intensity of the control cells and the closed circles are the QDs, respectively. Each Graph in *right lanes* shows the logarithmic scales corresponding to the *left* ones. The data are presented as means ± standard deviation. (B) EL-4 cells were stimulated with QDs at 0.1 mg/ml concentration. The cells were incubated for 1, 3, 5, 7, and 10 days. The cells were harvested, stained with propidium iodide for detection of dead cells, and observed by flow cytometry and fluorescent microscopy, as in Fig. 1. The fluorescence intensity of the QD-holding cells in 10^6-collected cells was measured by flow cytometric analysis and the cell population in each region was calculated by CytoAce300 analyzer (JASCO).

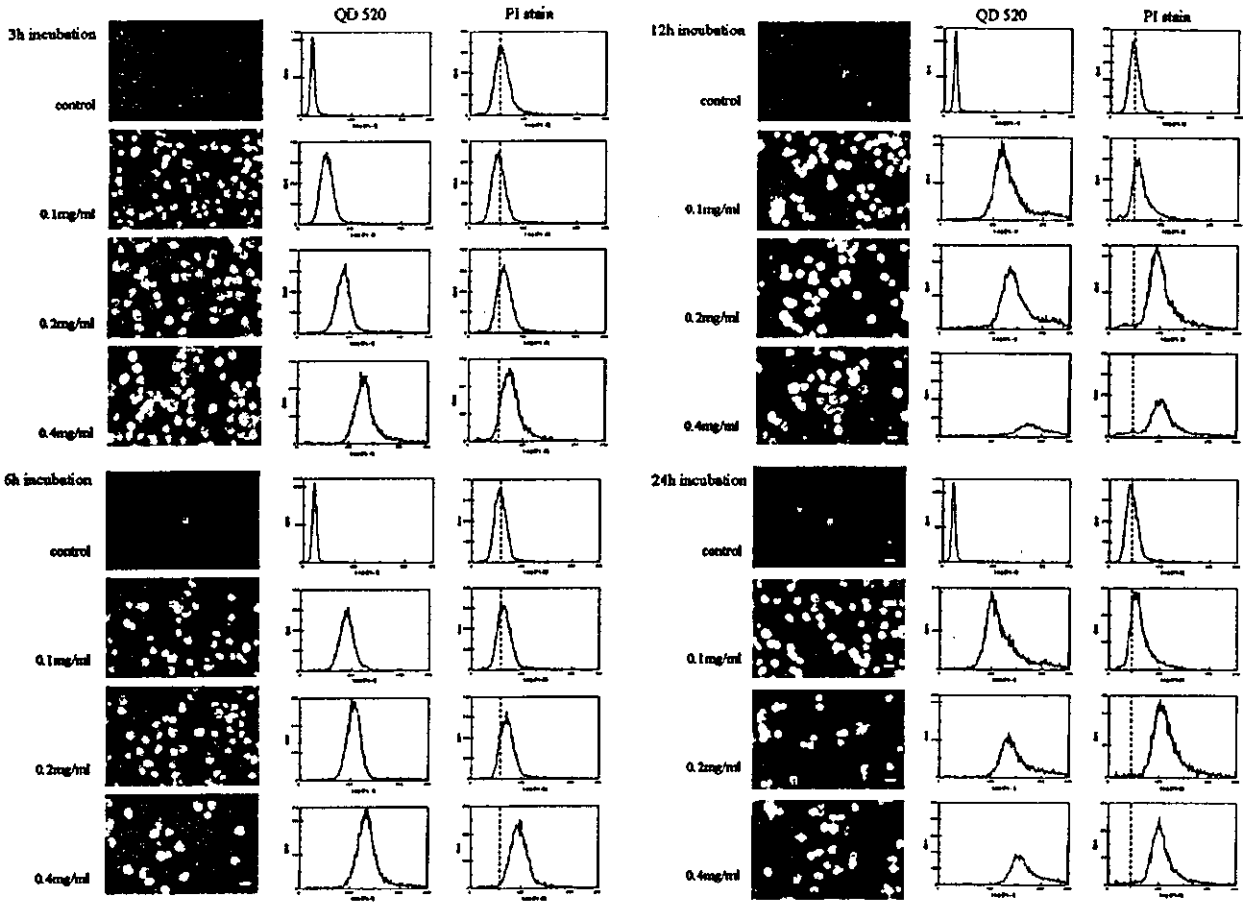

Fig. 2. The cytotoxicity of albumin-conjugated QDs depends on the QD-concentration. EL-4 cells were stimulated with culture media alone or with albumin-conjugated QD at the concentration of 0.1, 0.2, and 0.4 mg/ml. Cells were incubated for 3, 6, 12, and 24 h at 37 °C. The cells were harvested, stained for observation of dead cells, and measured by flow cytometric analysis. Fluorescence was measured by flow cytometry using an argon laser (488 nm). Detection was triggered by forward-angle light scattered signals. In the *graphs*, the relative cell number is given on the *y*-axis and the fluorescence intensity of QDs on the *x*-axis. Dotted lines in the *graphs* indicate the fluorescence medium of the unstimulated cells.

in 0.1 mg/ml concentration (Fig. 3A, upper graphs). Whereas the growth of both cells conformed to logarithmic growth phase, the doubling-time of QD-labeled cells was about 24 h and took 4 h longer than unlabeled cells (approximately 20 h). The fluorescence intensity of QD-labeled cells was logarithmically attenuated, but the attenuation ratio became lower after 24 h incubation (Fig. 3A, lower right). Moreover, the QDs that remained in the cells could be observed for more than a week (Fig. 3B). Approximately 10% of the cells still held QDs after 10 days culture, but fluorescent intensity of cells gradually decreased and highly concentrated in endosomes. This concentration of QDs was compatible with our previous study in Vero cells [17], implying that this labeling of cells by QDs could be applied not only adherent cell but also the cells that have the property of less endocytotic action and high-proliferation rate cells such as lymphocytes.

It is known that T cells were activated with various immune stimulants. Then, we investigated whether labeling of QDs held in the cells would be influenced by those stimulations. EL-4 cells were exposed to various stimulants after labeling of QDs. After stimulation, EL-4 cells were highly aggregated by stimulation with ConA and PHA. But no significant change was observed by stimulating for 24 h (Fig. 4). These results suggest that labeling of QDs were stable, and were not affected by either cell activation or cell function.

Then we compared the fluorescence of QD with those of other organic probes at the points of fluorescence intensity and photostability. Shown in Fig. 5A, fluorescence intensity of both QD and organic probes was approximately equivalent in the moment of excitation in the case of flow cytometric analysis. However after long-term exposure, e.g., long time observation using microscopes, fluorescence from organic probes w' , eliminated rapidly and almost disappeared within a minute (Fig. 5B). In contrast, the QDs kept emitting bright fluorescence for more than 30-min continuously (Fig. 5C).

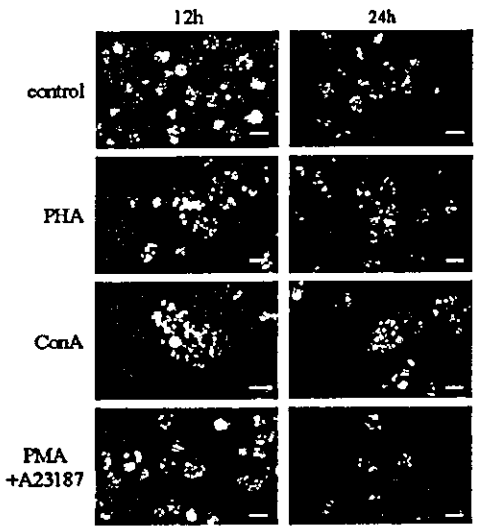

Fig. 4. Fluorescence of QDs was stable against activation of EL-4 cells. EL-4 cells were incubated with QD at 0.1 mg/ml concentration for 3 h. Then the cells were washed twice with DMEM and stimulated with 1 μg/ml ConA, 5 μg/ml PHA, and both 10 ng/ml PMA and 1 μM A23187. The cells were collected 12 and 24 h after stimulation. The cells were observed using a fluorescent microscopy, as in Fig. 1.

Next we considered the survival of QD-labeled cells in vivo. The cells labeled by QDs were intravenously injected into mice. The cells injected into mice were observed in the peripheral blood for 5 days after injection by microscopic analysis (Fig. 6). The fluorescence of QD-labeled cells was also observed until 5 days after injection, but the fluorescence intensity of cells was much smaller than expected. Unfortunately, fluorescence of PKH-dye was observed from cells by using neither microscopy nor flow cytometric analysis (data not shown). However, approximately 70% of QD-labeled cells were eliminated from blood circulation within 2 h after injection. We assumed that the excess number of QD-labeled cells would be homing on the other lymphatic tissue, as T-cell population in whole peripheral blood usually remained at approximately 20%. As expected, many cells including QDs were observed in spleen sections at 2 h after injection (Fig. 7A). In 2 h images, QD-labeled cells remained in the fringe area of white pulp and red pulp. After 5 days, fluorescence emitted from QDs was located in white pulp area. This result concurs with the fact that T-lymphocytes were first observed in red pulp and then moved and then

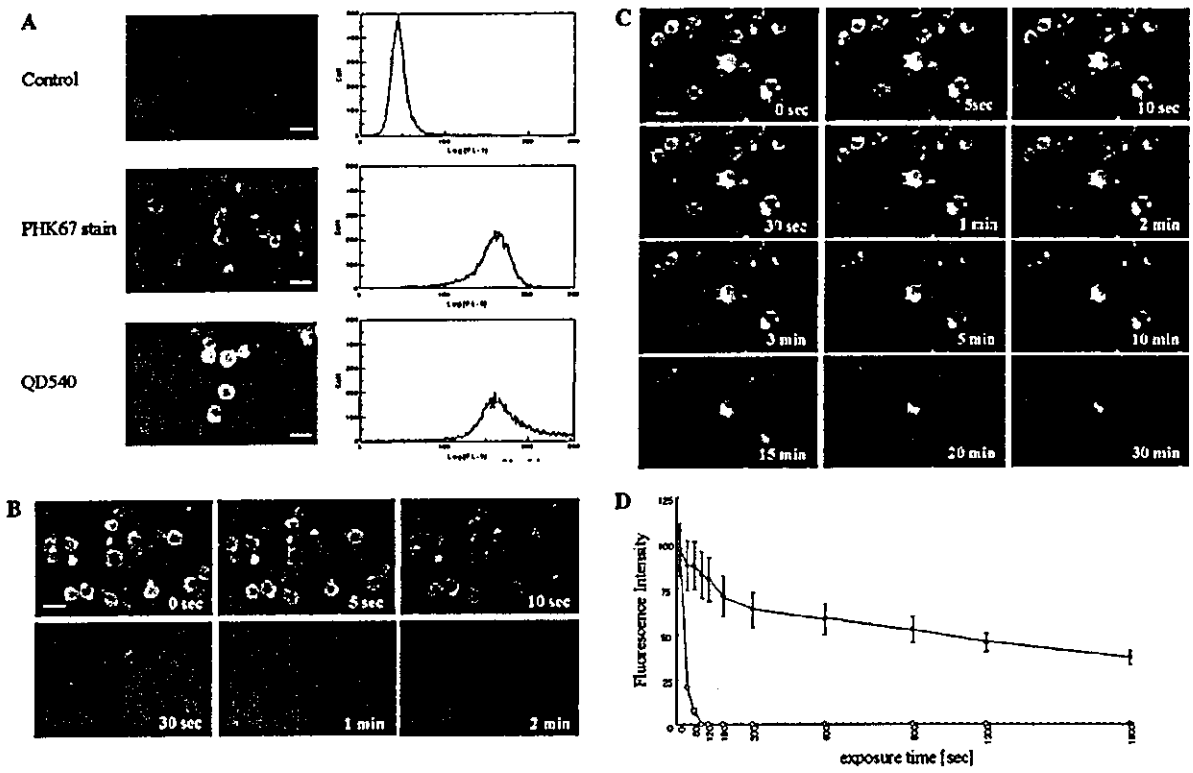

Fig. 5. Fluorescence of QDs was superior to that of organic flourophores with respect to the fluorescent lifetime. (A) Cells stained with QDs and organic dyes were observed by fluorescent microscopy and flow cytometric analysis. The cells were harvested, stained, and analyzed by flow cytometry and fluorescent microscopy, as in Fig. 1. (B) Observation of photostability of organic probe (PHK67). The cells were continuously excited and images were taken using D1X digital camera equipped with fluorescence microscope IX-81 at the indicated time by a 1.0 s exposure. Other conditions were the same as described in Fig. 1. (C) The photostability of QDs, as described in (B). (D) Comparison of the relative fluorescence intensity between QDs and the organic probes. The snapshots shown in Figs. 3B and C were calculated using the histogram analysis of Adobe Photoshop 7.0. Open circles indicate organic probes and closed circles are the QDs, respectively.

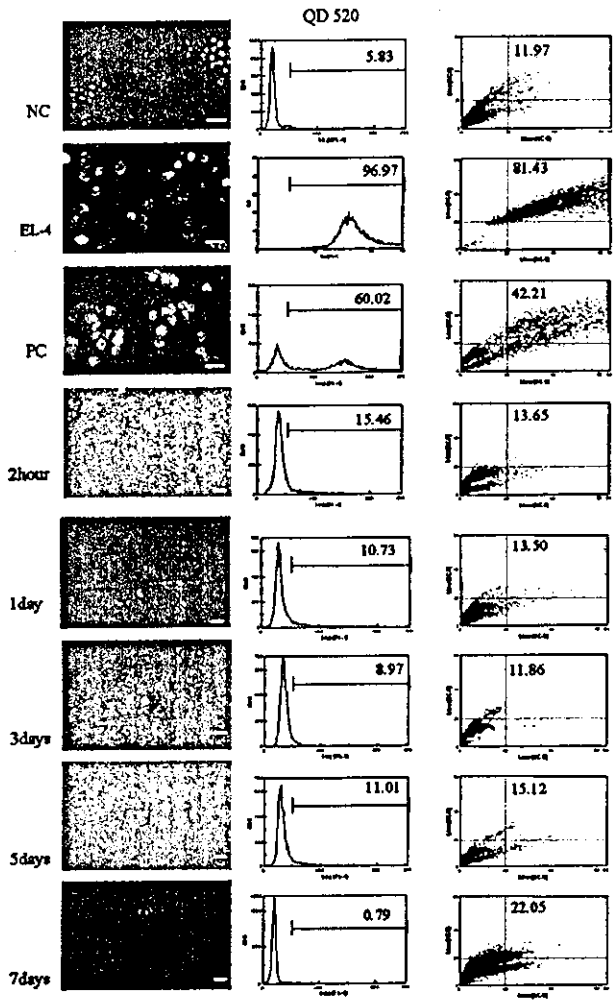

Fig. 6. Intravenously injected QD-labeled cells remained for several days in the peripheral blood. EL-4 cells used for administration were pre-stained with PKH26 Red Fluorescent Cell Linker Kit (Sigma) before incubated with 0.1 mg/ml QD. Then the cells were collected and re-suspended in serum-free DMEM and intravenously injected into the mice. The mice were sacrificed at indicated days ($n = 2$). The fluorescence intensity of the QD-holding cells was measured and calculated by a CytoAce300 analyzer, as shown in Fig. 3. In the *right graphs*, the forward scattered is given on the *y*-axis and side scattered on the *x*-axis. Shown numbers in inset mean the percentage of cells in upper right region of graphs. As positive control, an equivalent number of QD-labeled cells were added into the blood separately.

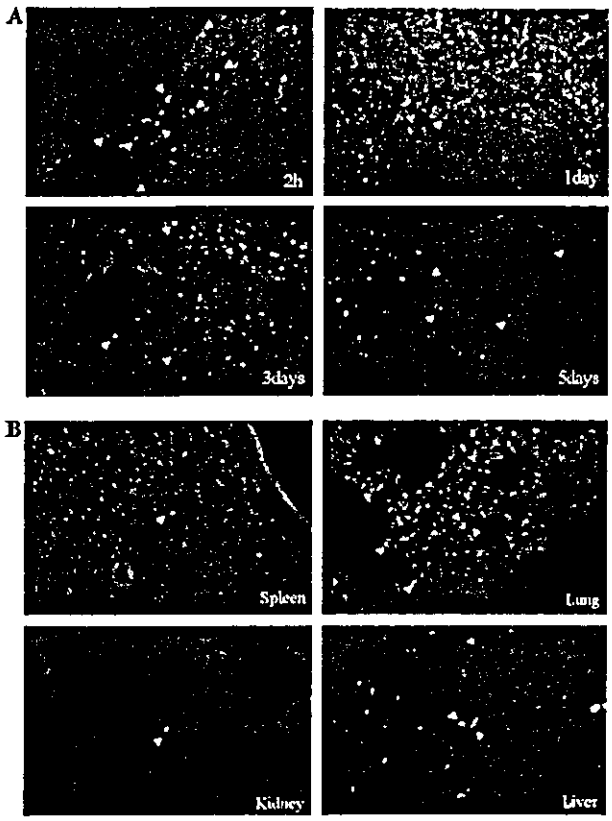

Fig. 7. QD-labeled EL4 was located into kidney, liver, lung, and spleen. (A) The fluorescence images of sliced spleen collected 2 h, 1 day, 3 days, and 5 days after administration ($n = 2$). (B) The fluorescence images of the kidneys, liver, lung, and spleen 7 days after administration. The cells were observed by fluorescence microscopy, as in Fig. 1. Arrowheads indicate the location of QD-holding cells.

accumulated in the splenic white pulp. In addition, QD-labeled cells could be detected in sections of the kidneys, liver, and lung in 7 days (Fig. 7B). The estimated value of QDs in each organ calculated in accordance with QDs contained in each section is shown in Table 1. This result suggests that approximately 20% of injected cells were present in those organs 7 days after injection.

Our results suggested that the QDs could be used as a cell-tracing marker, especially for that of the transplanted target cells. QDs could enable high luminescent labeling of target cells easily and these applications could also be applied to flow cytometric analysis. In this study, we performed the labeling of QDs in EL-4 lymphocytoma cell lines by cellular endocytotic pathways. This result indicated that it is possible to tag target cells only by adding albumin-conjugated QDs into the culture media. In addition, the injected QD-labeled cells were observed up to 5 days in this experiment. However, some of the QDs were eliminated from the cells after a long-time incubation time even in vitro, and the observed number of cells was smaller than expected; the number of cells observed 2 h after injection was quarter of the anticipated value and it decreased to 1/6 by next day. It was not elucidated in this research why QD labeled cells were disappearing from the body in these experiments, but we can presume three possibilities by our study. The first possibility was the attenuation of QDs from endosomes by cell division. As shown in Fig. 3, labeled QDs have already been detached in most of the labeled cells, even though a few QD-labeled cells remained for over a week in vitro. The fluorescence intensity of QD-labeled cell population was attenuated within first 24 h, but fluorescent attenuation ratio